GeroScience (2024) 46:2697–2714
https://doi.org/10.1007/s11357-023-01038-3

ORIGINAL ARTICLE

PEDF protects retinal pigment epithelium from ferroptosis and ameliorates dry AMD-like pathology in a murine model

Wei Xiang · Longhui Li · Qin Zhao · Yongcheng Zeng · Jinhui Shi · Zitong Chen · Guoquan Gao · Kunbei Lai

Received: 6 June 2023 / Accepted: 5 December 2023 / Published online: 28 December 2023

Abstract Age-related macular degeneration (AMD) is the leading cause of irreversible vision damage among elderly individuals. There is still no efficient treatment for dry AMD. Retinal pigment epithelial (RPE) degeneration has been confirmed to play an important role in dry AMD. Recent studies have reported that ferroptosis caused by iron overload and lipid peroxidation may be the primary causes of RPE degeneration. However, the upstream regulatory molecules of RPE ferroptosis remain largely unknown. Pigment epithelium-derived factor (PEDF) is an important endogenic protective factor for the RPE. Our results showed that in the murine dry AMD model induced by sodium iodate (SI), PEDF expression was downregulated. Moreover, dry AMD-like pathology was observed in PEDF-knockout mice. Therefore, the aim of this study was to reveal the effects and mechanism of PEDF on RPE ferroptosis and investigate potential therapeutic targets for dry AMD. The results of lipid peroxidation and transmission electron microscope showed that retinal ferroptosis was significantly activated in SI-treated mice and PEDF-knockout mice. Restoration of PEDF expression ameliorated SI-induced retinal dysfunction in mice, as assessed by electroretinography and optical coherence tomography. Mechanistically, western blotting and immunofluorescence analysis demonstrated that the overexpression of PEDF could upregulate the expression of glutathione peroxidase 4 (GPX4) and ferritin heavy chain-1 (FTH1), which proved to inhibit lipid peroxidation and RPE ferroptosis induced by SI. This study revealed the novel role of PEDF in ferroptosis inhibition and indicated that PEDF might be a potential therapeutic target for dry AMD.

Keywords Pigment epithelial-derived factor · Ferroptosis · Age-related macular degeneration · Retinal pigment epithelium

Wei Xiang and Longhui Li contributed equally to this study

Supplementary Information The online version contains supplementary material available at https://doi.org/10.1007/s11357-023-01038-3.

W. Xiang
Department of Clinical Laboratory Medicine, Guangdong Provincial People's Hospital (Guangdong Academy of Medical Sciences), Southern Medical University, Guangzhou, China

L. Li · Q. Zhao · Z. Chen · K. Lai (✉)
State Key Laboratory of Ophthalmology, Zhongshan Ophthalmic Center, Sun Yat-Sen University, Guangdong Provincial Key Laboratory of Ophthalmology and Visual Science, Guangdong Provincial Clinical Research Center for Ocular Diseases, Guangzhou, China
e-mail: laikunbei888@mail.sysu.edu.cn

Y. Zeng · J. Shi · G. Gao (✉)
Department of Biochemistry and Molecular Biology, Zhongshan School of Medicine, Sun Yat-Sen University, Guangzhou, China
e-mail: gaogq@mail.sysu.edu.cn

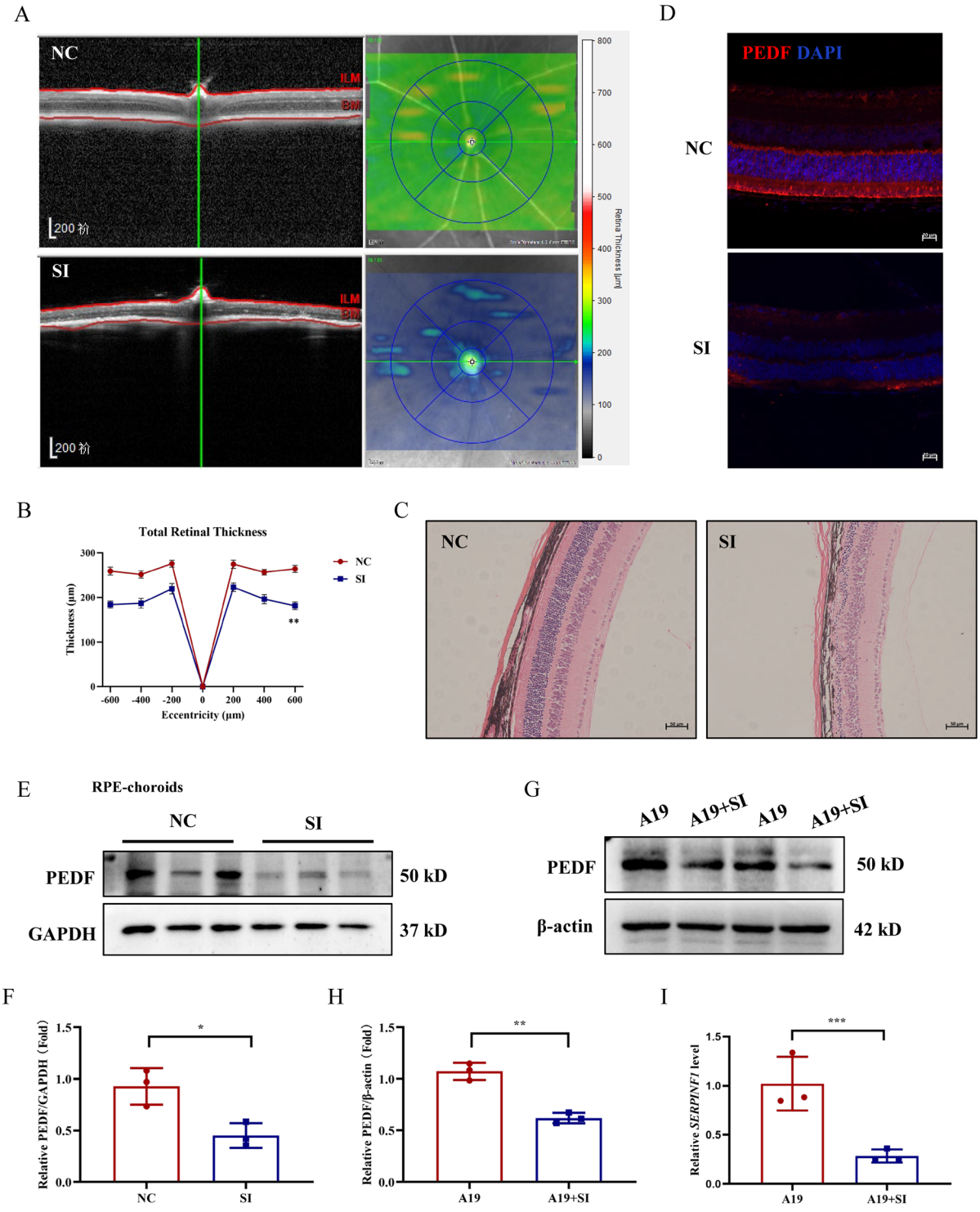
A
NC
ILM
BM
200 μm
SI
ILM
BM
200 μm
800
700
600
500
400
300
200
100
0
Retina Thickness [μm]
D
PEDF DAPI
NC
SI
B
Total Retinal Thickness
Thickness (μm)
300
200
100
0
-600 -400 -200 0 200 400 600
Eccentricity (μm)
NC
SI
**
C
NC
SI
E
RPE-choroids
NC
SI
PEDF
50 kD
GAPDH
37 kD
G
A19
A19+SI
A19
A19+SI
PEDF
50 kD
β-actin
42 kD
F
Relative PEDF/GAPDH (Fold)
1.5
1.0
0.5
0.0
*
NC
SI
H
Relative PEDF/β-actin (Fold)
1.5
1.0
0.5
0.0
**
A19
A19+SI
I
Relative SERPINF1 level
1.5
1.0
0.5
0.0
***
A19
A19+SI

◂**Fig. 1** The expression of PEDF decreased in SI-treated mice and ARPE-19 cell line. **A** Representative SD-OCT images in normal control and SI-treated mice. **B** Quantification of the relative ILM-RPE thickness from SD-OCT images of retinal sections. **C** H&E staining for retina morphological changes in normal control and SI-treated mice. Scale bar = 50 μm. **D** PEDF (red) immunostaining of retinas in normal control and SI-treated mice. Scale bar = 20 μm. **E** Protein levels of PEDF in the RPE-choroidal tissues of normal control and SI-treated mice. **F** Quantification of the PEDF expression in the RPE and choroidal tissues. **G** Protein levels of PEDF in ARPE-19 cells treated with or without 5 mM SI for 24 h. **H** Quantification of the PEDF expression in ARPE-19 cells. **I** Relative mRNA levels of *SERPINF1* in ARPE-19 cells treated with or without 5 mM SI for 24 h. SD-OCT, spectral-domain optical coherence tomography; ILM, internal limiting membrane; NC, normal control; $^{*}P < 0.05$, $^{**}P < 0.01$, $^{***}P < 0.001$

Introduction

Age-related macular degeneration (AMD) is the leading cause of irreversible vision damage among elderly individuals. The global prevalence of AMD is approximately 8.7%, and it is estimated that up to 288 million individuals globally will have AMD in 2040 [1]. AMD is commonly classified as dry AMD and wet AMD according to different pathological features. The proportion of patients with dry AMD was approximately 90% [2]. However, there is still no efficient treatment for dry AMD. Thus, it is essential to further explore the mechanism of dry AMD and identify potential therapeutic targets.

Retinal pigment epithelial (RPE) dysfunction is critical for the onset and development of AMD [3]. However, the causes and mechanisms of RPE dysfunction are still not fully understood. Ferroptosis, a newly discovered programmed cell death pathway, has been reported to be associated with the pathogenesis of RPE dysfunction in AMD [4–6]. The occurrence of ferroptosis depends on iron overload and lipid peroxidation [7, 8]. Recent studies have shown that antioxidants inhibit ferroptosis in RPE cells, providing new directions for the treatment of AMD [9]. However, there is controversy about the strategy to inhibit ferroptosis, and there is a lack of effective and biosafe targets to inhibit RPE ferroptosis.

Pigment epithelium-derived factor (PEDF), a secreted glycoprotein, is a member of the serine protease family encoded by the *SERPINF1* gene. PEDF was first found in RPE cell culture medium and has various functions, such as fibrosis and angiogenesis inhibition [10]. In retinas, PEDF has been shown to inhibit angiogenesis and protect the retina from oxidative stress injury [11–13]. It has also been reported to have a regulatory effect on lipid metabolism, and its reduction leads to increased fatty acid uptake and lipid droplet formation [14]. However, the relationship between PEDF and ferroptosis has not been determined.

This study aimed to explore the effect and mechanism of PEDF in sodium iodate (SI)-induced ferroptosis and evaluate the potential of PEDF for dry AMD treatment. Briefly, ferroptosis was activated in PEDF-knockout mice, as evidenced by lipid reactive oxygen species (ROS) accumulation and the downregulated expression of ferroptosis inhibitors, including glutathione peroxidase 4 (GPX4) and ferritin heavy chain-1 (FTH1). Moreover, the restoration of PEDF expression ameliorated dry AMD-like pathology in a mouse model induced by SI.

Methods

Cell culture, cell treatment, and cell transfection

ARPE-19 cells were purchased from the American Type Culture Collection. Dulbecco's modified Eagle's medium (Gibco, USA) containing 10% fetal bovine serum (FBS) (Sigma, USA) was used to culture ARPE-19 cells. Solid SI (Macklin, China) was dissolved in PBS to form a sterile 250 mM solution and then filtered for cell treatments. The cells were exposed to 5 mM SI or PBS for 24 h. The PEDF overexpression plasmid used the pCDNA-3.1(+) vector with a human cytomegalovirus immediate-early promoter for high-level expression in a wide range of mammalian cells. Then the pCDNA3.1-PEDF plasmid and pCDNA3.1 plasmid were used as a template to synthesis adenoviruses. The PADV-mCMV-PEDF-3FLAG adenovirus (Ad-PEDF) and the control adenovirus (Ad-Ctrl) were obtained from Obio Technology (China). The PEDF adenovirus titer was 6.32×10^{10} PFU/mL, and the control adenovirus titer was 10^{11} PFU/mL. When cell grew at the confluency of 70–80%, the transient transfection of PEDF overexpression adenovirus or control adenovirus was carried out according to the manufacturer's instructions.

Animals model

The animal experiments were approved by the Animal Care Committee of Sun Yat-Sen University

(approval number: SCYK2016-0029). Guangdong Provincial Animal Center (Guangzhou, China) provided the C57BL/6 mice, while PEDF homozygous KO (PEDF$^{-/-}$) mice were provided by Dr. S.J. Wiegand of Regeneron Pharmaceuticals, Inc. (Tarrytown, NY).

Sodium iodate treatment

Six- to eight-week-old C57BL/6 J mice were fed in a specific pathogen-free (SPF) environment and maintained on a 12-h light/dark cycle. Solid sodium iodate (SI) was dissolved in PBS to form a sterile 1 mg/ml

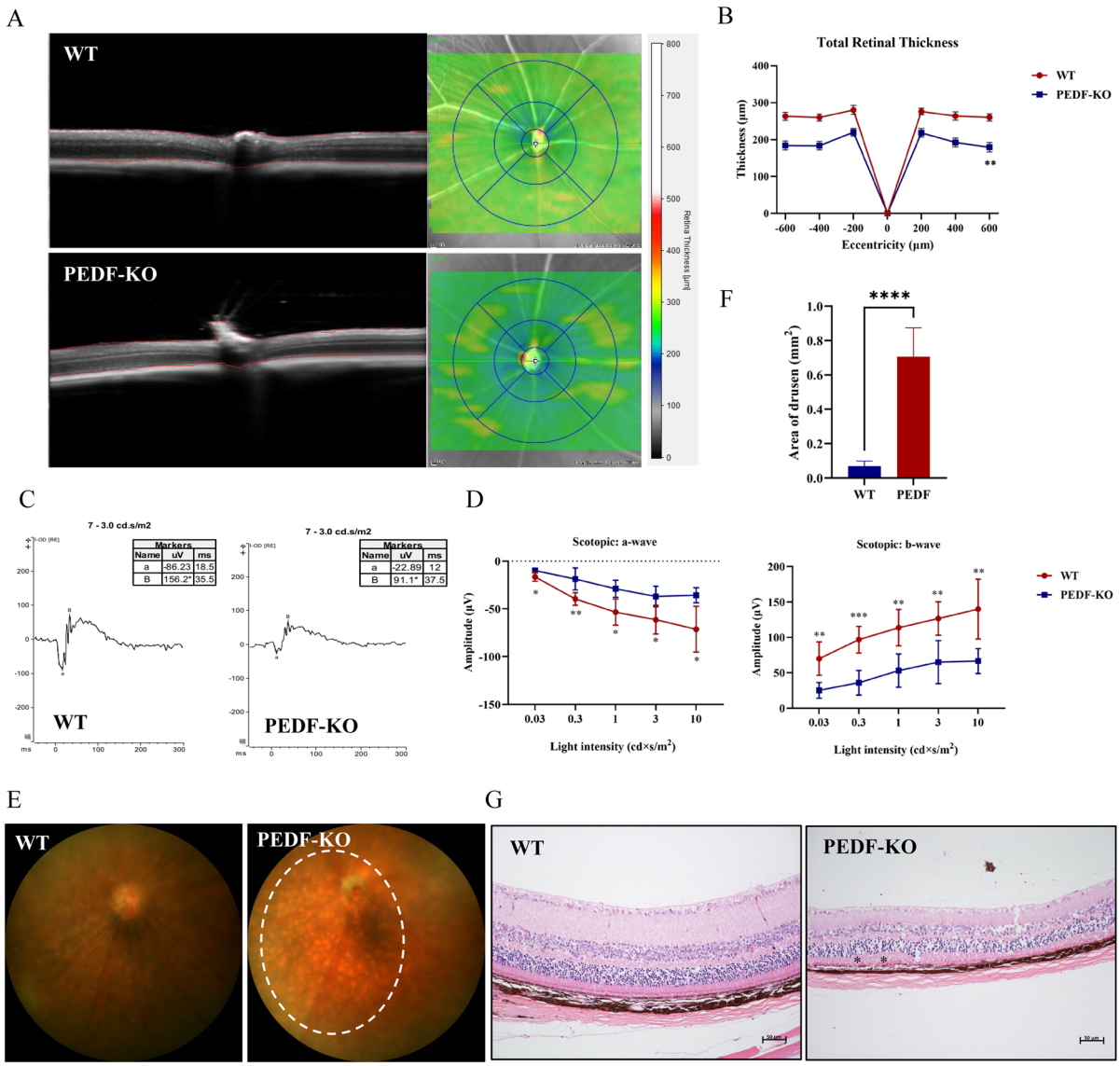

Fig. 2 PEDF-KO mice appeared AMD like retinopathy. **A** Representative SD-OCT images in the WT and PEDF-KO mice. **B** Quantification of the relative ILM-RPE thickness from SD-OCT images. **C** Representative scotopic-ERG a- and b-wave by full-field ERG in the WT and PEDF-KO mice. **D** Quantification of the scotopic-ERG a- and b-wave amplitude values by full-field ERG. **E** Fundus photograph of the WT and PEDF-KO mice. **F** Quantification of the drusen in the WT and PEDF-KO mice. **G** H&E staining for retina morphological changes in WT and PEDF-KO mice. Scale bar = 20 μm. SD-OCT, spectral-domain optical coherence tomography; ILM, internal limiting membrane; WT, wild type; PEDF-KO, PEDF-knockout. $^{*}P < 0.05$, $^{**}P < 0.01$, $^{***}P < 0.001$

solution and then filtered for tail vein injection [15]. The mice were intravenously injected with the SI solution at a dose of 30 mg/kg, and the control group received an equivalent volume of PBS.

Intravitreal injection of adenoviruses

The mice were anesthetized with 10% chloral hydrate (50 µl/10 g). Then, the mice were treated with 0.5% compound tropicamide eye drops and 1% carboxymethylcellulose sodium eye drops to keep their eyes dilated and moist. Two microlitres of PEDF or control adenovirus was injected into one eye of each mouse using an ultrafine 33-g Hamilton syringe. The intravitreal injection was gently performed, and the needle was held in place for 1 min to allow the adenovirus to spread in the vitreous. Tobramycin dexamethasone eye ointment was applied to the injection site, and the mice were allowed to recover from anesthesia in an electric heating blanket.

Electroretinography

The mice were anesthetized with 10% chloral hydrate (50 µl/10 g). Then, the mice were treated with 0.5% compound tropicamide eye drops and 1% carboxymethylcellulose sodium eye drops to keep their eyes dilated. We used Celeris (Diagnosys, USA) to detect and record electroretinography (ERG) responses. In response

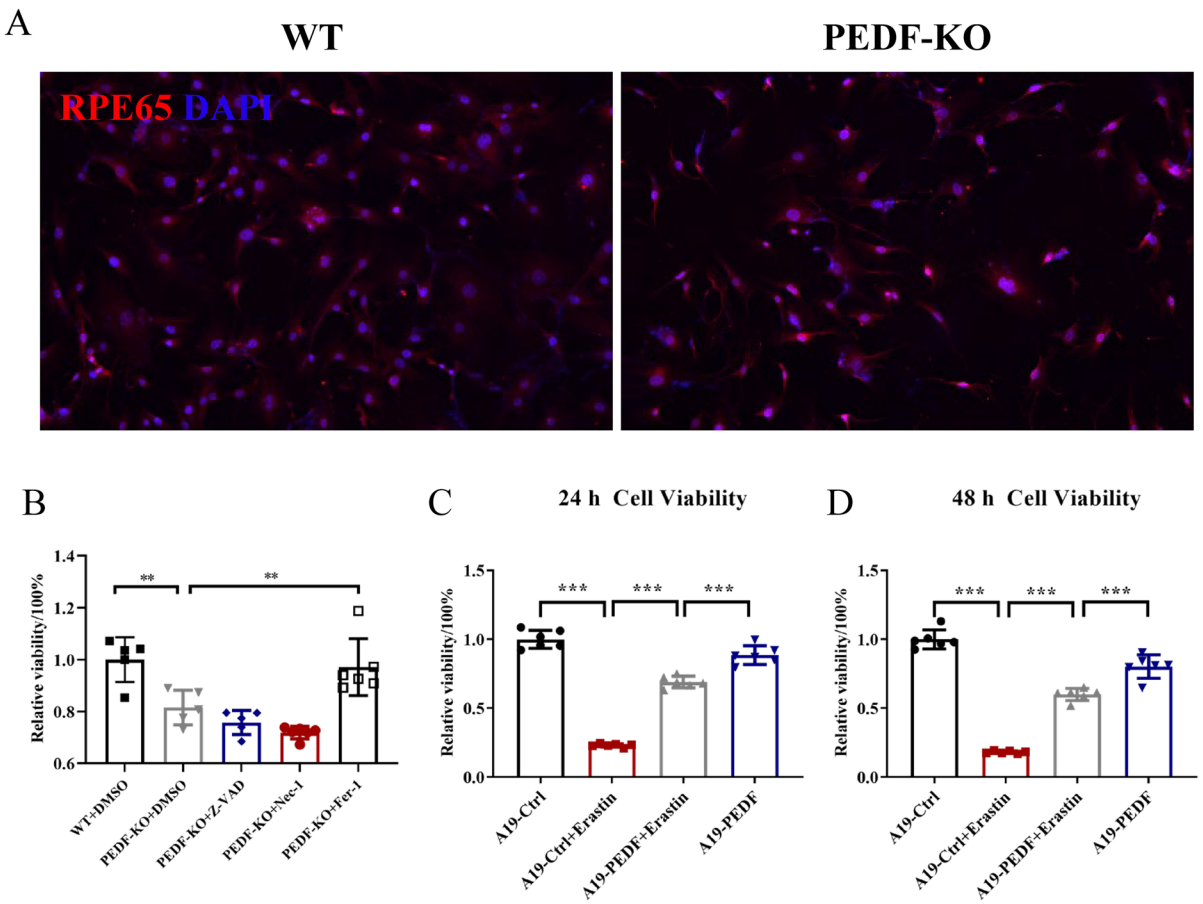

Fig. 3 The screening of ferroptosis, apoptosis, and necroptosis in primary RPE extracted from PEDF-KO mice. **A** RPE65 (red) immunostaining to identify the primary mouse RPE cells. **B** Cell viability detected by CCK-8 assay in primary RPE cells cultured from WT or PEDF-KO mice treated with DMSO, 20 µM Z-VAD (apoptosis inhibitor), 40 µM Nec-1 (necroptosis inhibitor) or 4 µM Fer-1 (ferroptosis inhibitor). **C**, **D** Cell viability detected by CCK-8 assay in PEDF-expressing ARPE-19 cells treated with 10 uM erastin (ferroptosis activator) for 24 h (**C**) and 48 h (**D**). ***$P < 0.001$

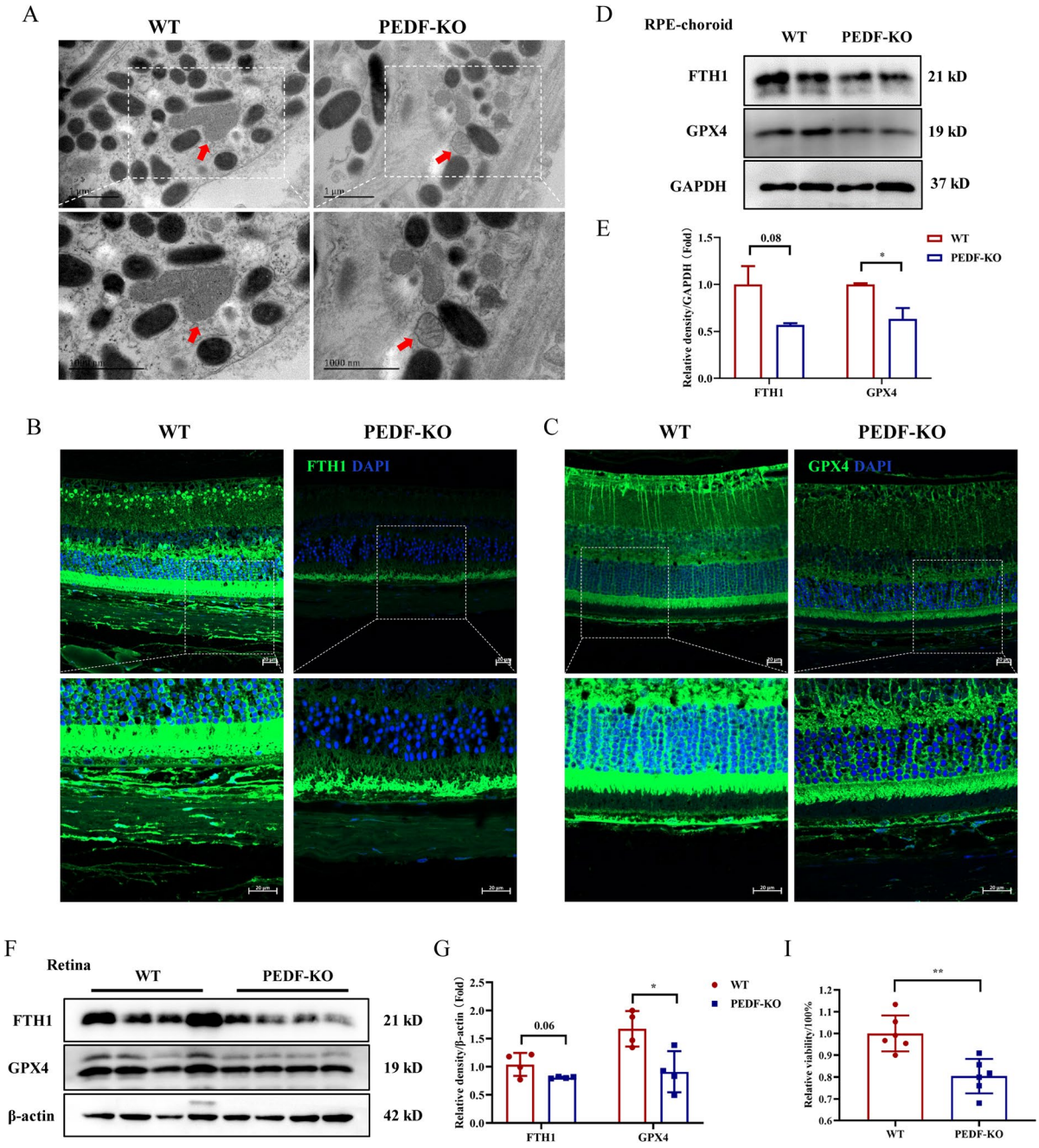

Fig. 4 PEDF deficiency triggered ferroptosis in the RPE of mouse. **A** Ultrastructure of mitochondria in RPEs from WT or PEDF-KO mice was imaged by TEM. Red arrowheads indicate mitochondria. Scale bars = 1 μm. **B**, **C** FTH1 (green) (**B**) and GPX4 (green) (**C**) immunostaining of retinas in the WT and PEDF-KO mice. Scale bar = 20 μm. **D** Protein levels of FTH1, GPX4 in the RPE and choroidal tissues of WT or PEDF-KO mice. **E** Quantification of the FTH1, GPX4 expression in RPE and choroid tissues. **F** Protein levels of FTH1, GPX4 in the retinas of WT or PEDF-KO mice. **G** Quantification of protein levels of FTH1, GPX4 in retinas. **H** Lipid ROS levels detected by BODIPY™ 581/591 C11 staining in primary RPE cells cultured from WT or PEDF-KO mice. Scale bar = 20 μm. **I** Cell viability detected by CCK8 assay in primary RPE cells cultured from WT or PEDF-KO mice. **J** Western blot analysis of GPX4, FTH1 in primary RPE cells cultured from WT or PEDF-KO mice. **K** Quantification of the FTH1, GPX4 expression in primary RPE cells cultured from WT or PEDF-KO mice. **L** mRNA levels of *Gpx4*, and *Fth1* in primary RPE cells cultured from WT or PEDF-KO mice. WT, wild type; TEM, transmission electron microscope; ROS, reactive oxygen species; $^{*}P < 0.05$, $^{**}P < 0.01$

to different intensities of white light flashes, the corneal ERG electrodes were adjusted to record the ERG.

Fundus photography

After the mice were anesthetized, the eyes were dilated with 0.5% compound tropicamide, and the cornea was moistened with 1% carboxymethylcellulose sodium eye drops. A retinal imaging system (Phoenix, MicronIV, USA) was used to capture the fundus images. The fundus images of mice were processed with ImageJ (version 1.54d, National Institute of Health, USA). First, we defined a scale bar for all the images. Then, the images were converted to 8-bit type. Finally, the area of drusen was measured after the drusen regions were manually surrounded.

Optical coherence tomography

Optical coherence tomography (OCT) was performed after fundus photography using a modified Spectralis Heidelberg Engineering system (Heidelberg, Germany). The mice were administered an additional 1% carboxymethylcellulose sodium eye drop and were positioned on a custom holder to maintain eye moisture. We used the pattern of the standard 30° field to obtain the images and analyzed the images with Eye Explorer software version 1.9.14.0 (Heidelberg Engineering, Heidelberg, Germany). OCT imaging was conducted using a volume scan with 57 frames (ART), 786 A-scans, a 30°×25° field of view, 100 scans at Δ120 μm, and 5 scans per second. Tobramycin Eye ointment was applied to the eyes during recovery. Total retinal thickness at 200 μm, 400 μm, and 600 μm, centered on the murine optic papilla, was measured using ImageJ (version 1.54d, National Institute of Health, USA).

Transmission electron microscope

RPE and choroidal tissues were fixed in 2.5% glutaraldehyde and 150 mM sodium cacodylate overnight at 4 °C. The tissues were then postfixed in 1% OsO_4 and uranyl acetate before being dehydrated in ethanol and embedded in epoxy resin. Ultrathin sections were placed on formvar-coated grids, stained with uranyl acetate and lead citrate and examined using a transmission electron microscope (TEM) (Tecnai Spirit, Netherlands).

Isolation and culture of primary mouse RPE cells

All surgical instruments were disinfected in advance using 75% alcohol and UV radiation. Suckling mice were anesthetized and immersed in 75% alcohol to ensure sterility. The eyeballs were carefully enucleated and placed in DMEM containing 1%

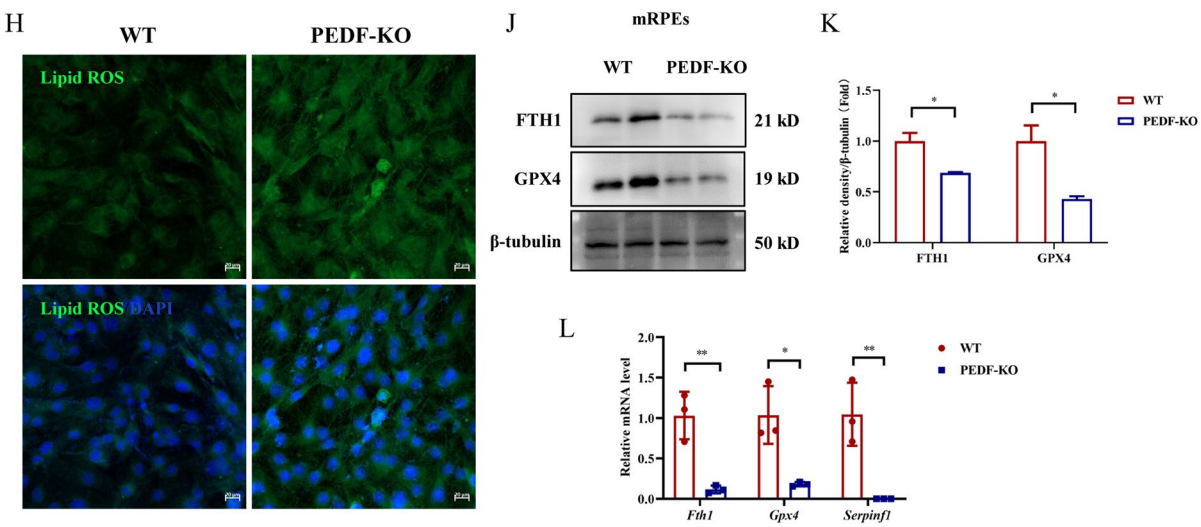

Fig. 4 (continued)

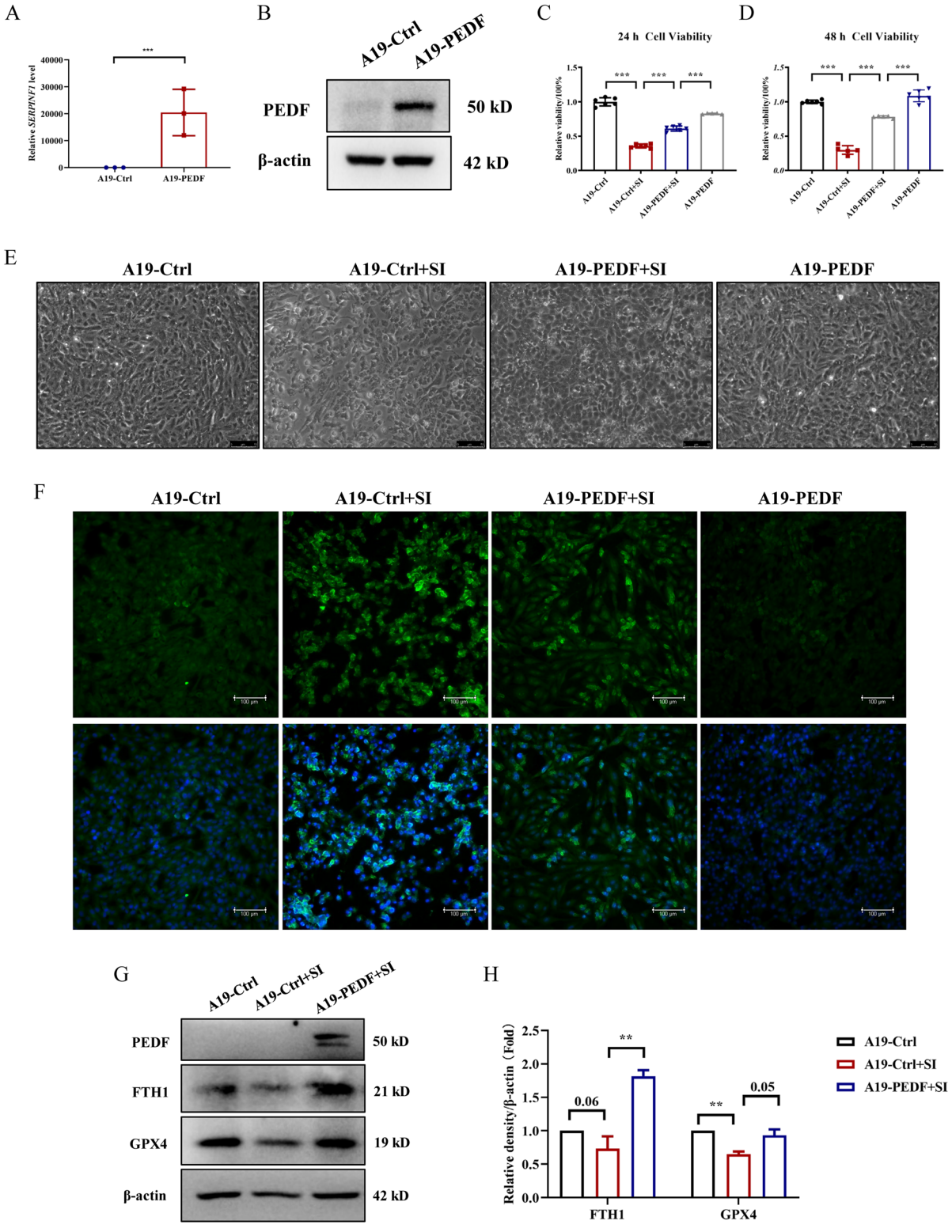
A
Relative SERPINF1 level
40000
30000
20000
10000
0
***
A19-Ctrl
A19-PEDF
B
A19-Ctrl
A19-PEDF
PEDF
50 kD
β-actin
42 kD
C
24 h Cell Viability
Relative viability/100%
1.5
1.0
0.5
0.0
***
***
***
A19-Ctrl
A19-Ctrl+SI
A19-PEDF+SI
A19-PEDF
D
48 h Cell Viability
Relative viability/100%
1.5
1.0
0.5
0.0
***
***
***
A19-Ctrl
A19-Ctrl+SI
A19-PEDF+SI
A19-PEDF
E
A19-Ctrl
A19-Ctrl+SI
A19-PEDF+SI
A19-PEDF
F
A19-Ctrl
A19-Ctrl+SI
A19-PEDF+SI
A19-PEDF
G
A19-Ctrl
A19-Ctrl+SI
A19-PEDF+SI
PEDF
50 kD
FTH1
21 kD
GPX4
19 kD
β-actin
42 kD
H
Relative density/β-actin (Fold)
2.5
2.0
1.5
1.0
0.5
0.0
**
0.06
**
0.05
FTH1
GPX4
A19-Ctrl
A19-Ctrl+SI
A19-PEDF+SI

◂**Fig. 5** The overexpression of PEDF inhibited the ferroptosis triggered by SI in ARPE-19. **A**, **B** mRNA (**A**) and protein (**B**) levels of PEDF in PEDF-overexpressing ARPE-19 cells. **C**, **D** Cell viability detected by CCK-8 assay in PEDF-overexpressing ARPE-19 cells treated with 5 mM SI for 24 h (**C**) and 48 h (**D**). **E** Cell morphology change in PEDF-overexpressing ARPE-19 cells treated with 5 mM SI for 24 h. **F** Lipid ROS levels detected by BODIPY™ 581/591 C11 staining in PEDF-overexpressing ARPE-19 cells treated with 5 mM SI for 24 h. **G** Western blot analysis of PEDF, GPX4 and FTH1 in PEDF-expressing ARPE-19 cells treated with 5 mM SI for 24 h. **H** Quantification of the FTH1, GPX4 expression in PEDF-expressing ARPE-19 cells treated with 5 mM SI for 24 h. ***$P < 0.001$

penicillin−streptomycin for 4 h. The RPE and choroid layers were separated and subjected to digestion using collagenase IV (Sigma, USA) at 37 °C for 30 min. The digestion was terminated, and the cells were collected by centrifugation at a speed of 1000 rpm for 10 min. The isolated cells were then cultured in DMEM with 20% FBS and 1% penicillin−streptomycin.

Cell Counting Kit-8 assays

Cell Counting Kit-8 (CCK-8) assays were performed with kits from New Cell & Molecular Biotech (C6005). A total of 10^4 cells per well were seeded in 96-well plates and treated as indicated. Ten microlitres of CCK-8 solution was added to each well and then incubated for 1 h. A Sunrise microplate reader (Tecan, Austria) was used to assess cell viability at an absorbance of 450 nm.

Lipid reactive oxygen species detection

We detected live-cell fluorescence levels of lipid reactive oxygen species (ROS) using 5 μM C11-BODIPY (581/591). ARPE-19 or primary mouse RPE cells were resuspended in 100 μL of fresh Hank's balanced salt solution (HBSS), and then C11-BODIPY was added and incubated for 30 min. After the samples were washed three times in HBSS, intracellular lipid ROS were detected using a fluorescence microscope.

Western blot analysis

Tissues or cells were dissociated in RIPA lysis buffer (Beyotime, P0013B) containing the protease inhibitor phenylmethanesulfonyl fluoride (PMSF). A BCA Detection Kit (KeyGen Biotech, China) was used to quantify the protein concentrations of the lysates. The protein supernatants were denatured at 95 °C for 5 min. Equal amounts of protein were separated on an SDS–polyacrylamide gel and transferred to a polyvinylidene fluoride (PVDF) membrane. The PVDF membrane was blocked with 5% milk solution for one hour. Then, primary antibodies against the target proteins PEDF (Millipore, MAB-1059), GPX4 (Beyotime, AF7020), FTH1 (Beyotime, AF2104), β-actin (Sigma, A5441), β-tubulin (Abcam, ab188548), and GAPDH (Proteintech, 60004–1) were added and incubated overnight and secondary antibodies (anti-mouse or anti-rabbit) were added and incubated for four hours at 4 °C. Western enhanced chemiluminescence (ECL) substrate was added to develop chemiluminescence. The specific antibody information, such as dilution rate and product code, is summarized in Supplemental Table 1.

Tissue or cell histology and immunofluorescence analysis

For histological analysis, retinas were fixed in a solution of 4% paraformaldehyde before being frozen and sectioned. PBS was used to wash the sections, and then the sections were permeabilized using 0.1% Triton X-100 for 15 min. The sections were blocked with PBS containing 2% bovine serum albumin at 37 °C for 1 h. PEDF (Millipore, MAB-1059), GPX4 (Beyotime, AF7020), FTH1 (Beyotime, AF2104) and ZO-1 (Beyotime, AF8394) primary antibodies were applied to the tissues or cells and incubated overnight at 4 °C. After being washed three times in PBS, the sections were incubated with fluorescent secondary antibodies (anti-mouse or anti-rabbit) at 37 °C for one hour. Finally, the cell nuclei were counterstained using 4,6-diamidino-2-phenylindole (DAPI) at room temperature for 10 min. The specific antibody information, such as dilution rate and product code, is summarized in Supplemental Table 1.

Quantitative real-time PCR

An RNA Extraction Kit (EZB-RN001-plus, EZBioscience) was used to isolate RNA from cells. Then, the Primer ScriptTM RT Reagent Kit (RR047A, Takara) was used to reverse transcribe mRNA into cDNA. The mRNA levels were quantified by using SYBR® Green I Reagent (RR820A, Takara) and a Bio-Rad CFX96 Real-Time system. The levels of target mRNAs were normalized to the levels of β-actin

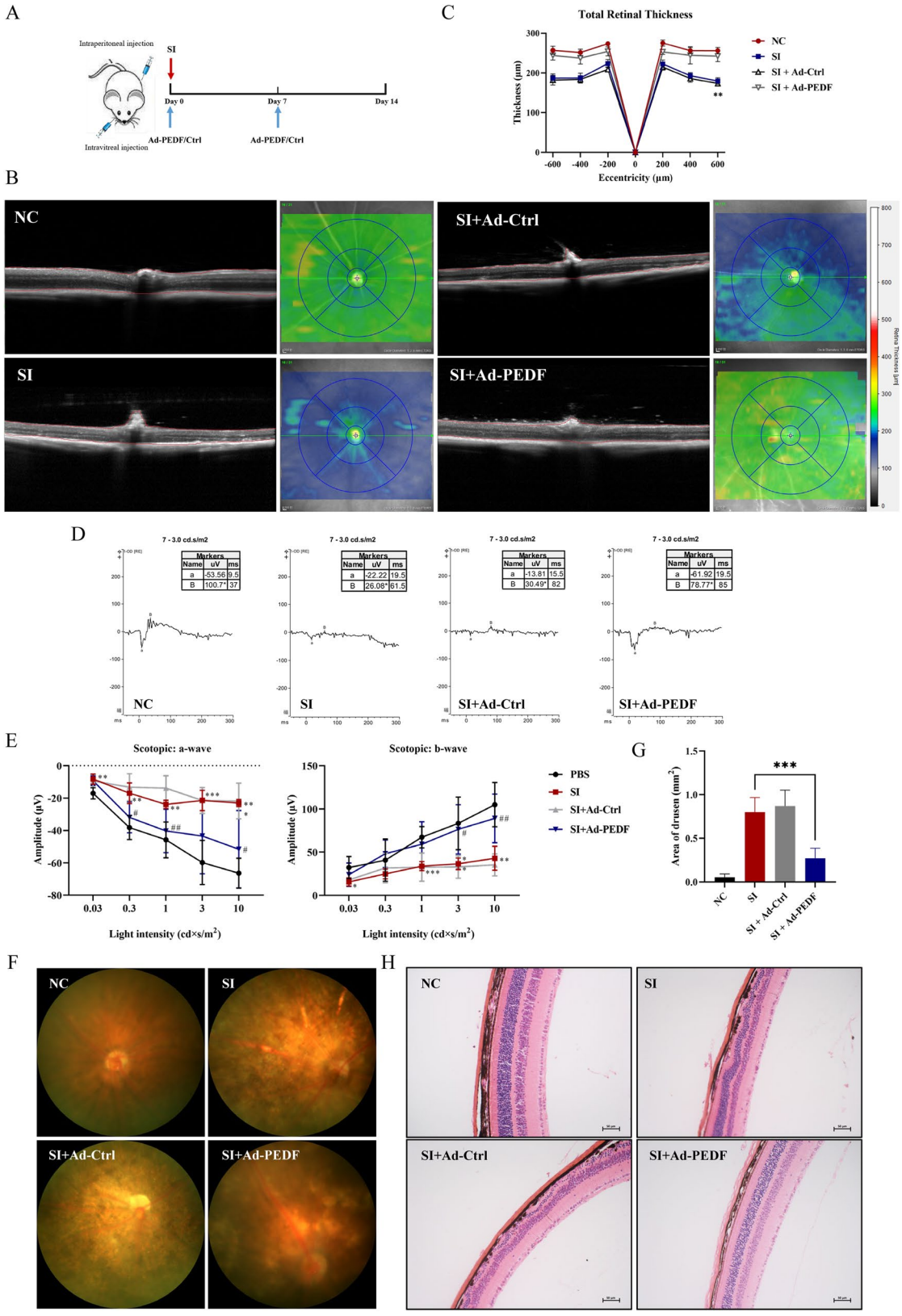
A
Intraperitoneal injection
SI
Day 0
Day 7
Day 14
Ad-PEDF/Ctrl
Ad-PEDF/Ctrl
Intravitreal injection
C
Total Retinal Thickness
Thickness (μm)
Eccentricity (μm)
NC
SI
SI + Ad-Ctrl
SI + Ad-PEDF
B
NC
SI+Ad-Ctrl
SI
SI+Ad-PEDF
D
7 - 3.0 cd.s/m2
NC
SI
SI+Ad-Ctrl
SI+Ad-PEDF
E
Scotopic: a-wave
Scotopic: b-wave
Amplitude (μV)
Light intensity (cd×s/m²)
PBS
SI
SI+Ad-Ctrl
SI+Ad-PEDF
G
Area of drusen (mm²)
F
NC
SI
SI+Ad-Ctrl
SI+Ad-PEDF
H
NC
SI
SI+Ad-Ctrl
SI+Ad-PEDF

◂ **Fig. 6** PEDF ameliorated SI-induced AMD-like retinopathy in mice. **A** Schematic diagram of the timepoint design for the AMD mouse model via SI tail-vein injection. PEDF-expressing adenovirus (Ad-PEDF) or control adenovirus (Ad-Ctrl) were intravitreally injected simultaneously, and the mouse retinas were collected at day 14 post-injection. **B** Representative SD-OCT images of the mice in different treatment groups. **C** Quantification of the relative ILM-RPE thickness from SD-OCT images of retinal sections. **D** Representative scotopic-ERG a- and b-wave amplitude by full-field ERG in different treatment groups. **E** Quantification of the scotopic-ERG a- and b-wave amplitude values by full-field ERG. **F** Fundus photograph of the mice in different treatment groups. **G** Quantification of the drusen in the mice in different treatment groups. **H** H&E staining for RPE pigmentation and morphological changes in the mice in different treatment groups. **I** ZO-1 (green) immunostaining of ARPE-19 cells in different treatment groups. SD-OCT, spectral-domain optical coherence tomography; ILM, internal limiting membrane; ERG, electroretinogram. $^{*}P < 0.05$, $^{**}P < 0.01$, $^{***}P < 0.001$

mRNA. The specific sequences of the primers are shown in Supplemental Table 2.

Statistical analysis

All values are reported as the mean ± SD. Data from more than two groups were compared using the Student-Newman−Keuls test. Two-tailed Student's *t* test was used to compare the means between two groups. A minimum of three independent experiments were conducted to verify the results. All analyses were performed using GraphPad Prism 8.0 (GraphPad Prism Software, CA, USA). A *P* value less than 0.05 (two-sided) was deemed statistically significant.

Results

The expression of PEDF was reduced in SI-induced AMD-like mice and RPE cells

RPE abnormalities were selectively induced by SI, and an RPE mouse oxidative stress model was established to mimic various symptoms of dry AMD, including drusen and photoreceptor degeneration [16, 17]. OCT images showed that SI induced thinning of the whole retina, which was shown by the thickness heatmap (Fig. 1A, B). Hematoxylin and eosin (H&E) staining showed that RPE cell arrangement was chaotic in the retinas of SI-treated mice (Fig. 1C). The results showed that SI successfully induced AMD-like symptoms in mice. To further examine the relationship between PEDF and AMD, we examined the expression of PEDF in SI-induced AMD-like mice. The immunofluorescence (IF) results showed that PEDF expression was decreased in SI-induced AMD-like mouse retinas compared with that in the normal control group (NC) (Fig. 1D). Furthermore, the western blot results indicated that PEDF expression was significantly decreased in SI-induced RPE and choroidal tissues (Fig. 1E, F). We further treated ARPE-19 cells with 5 mM SI and analyzed PEDF expression. The western blot and qRT−PCR results showed that SI treatment significantly decreased the protein and mRNA levels of PEDF (Fig. 1G–I). Therefore, the results indicated that a reduction in PEDF is involved in the onset of dry AMD.

PEDF deficiency triggered AMD-like retinopathy

To further understand the role of PEDF in AMD, we constructed PEDF-knockout mice. OCT images showed that PEDF deletion caused thinning of the whole retinal layer compared with that in WT mouse retinas (Fig. 2A, B). The ERG results showed that wild-type mice (WT) had a solid scotopic ERG curve, while PEDF-knockout mice had a substantially reduced ERG curve (Fig. 2C, D). The results indicated that PEDF deficiency induced retinal visual damage. Furthermore, we performed fundus photography, and the results indicated that PEDF-knockout mice had more drusen-like lesions (Fig. 2E, F). These data showed that PEDF deficiency strongly negatively affected the function of the retinal pigment epithelium and photoreceptors in vivo. We further tested the morphological characteristics of PEDF-knockout mice. H&E staining showed abnormal hypopigmentation and predominant loss of RPE cells in PEDF-knockout mouse retinas (Fig. 2G). All together, these results showed that PEDF deficiency triggered AMD-like retinopathy.

PEDF deficiency triggered ferroptosis in the mouse retina and ARPE-19 cells

To further understand the molecular mechanism that may result in these impairments, we found that recent studies reported that ferroptosis caused by iron

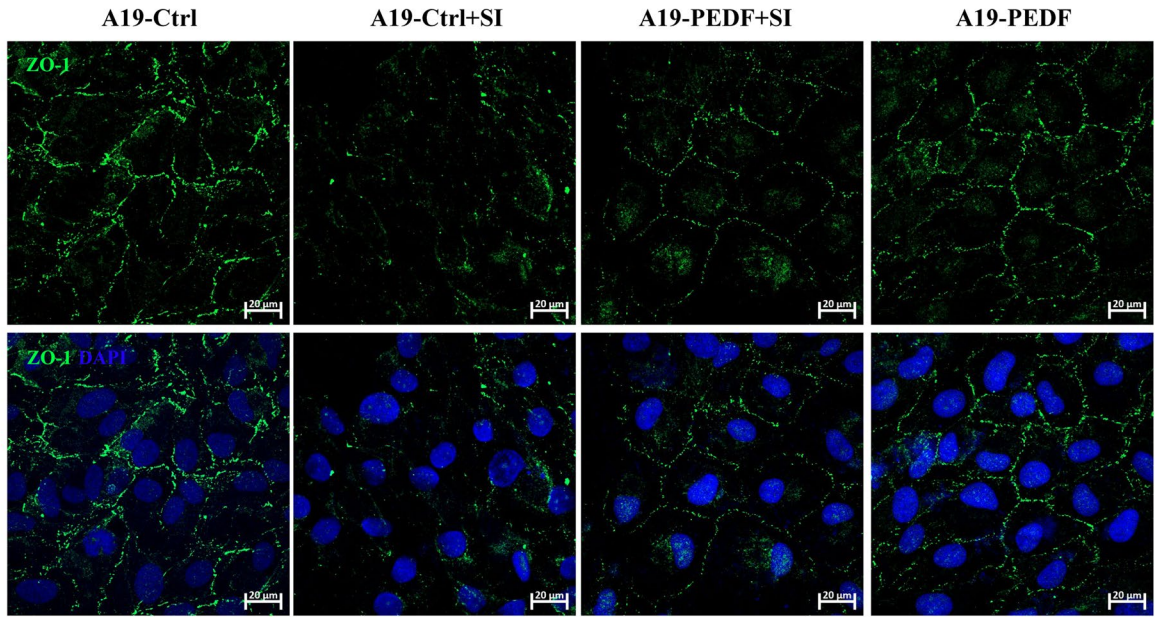

Fig. 6 (continued)

accumulation and lipid peroxidation was the main mechanism underlying RPE injury [5, 17]. PEDF was shown to be involved in lipid metabolism and the inhibition of oxidative stress [11–13]. We hypothesized that PEDF was involved in ferroptosis. Firstly, we cultured the primary mouse RPE cells to exclude pyroptosis and necrosis. The primary RPE cells from WT and PEDF-knockout mice were identified by positive expression of RPE65 (Fig. 3A). The CCK8 results indicated that the cell viability of PEDF-knockout primary RPE cells was rescued by the potent and selective ferroptosis inhibitor Ferrostain-1 (Fer-1), while the apoptosis inhibitor Z-VAD or necroptosis inhibitor Necrostatin-1 (Nec-1) had little effect on the PEDF-knockout primary RPE cells (Fig. 3B). Furthermore, we tested whether PEDF could rescue the cell viability induced by the specific ferroptosis activator (erastin). The CCK8 results indicated that PEDF overexpression significantly inhibited ferroptosis in 24 h or 48 h (Fig. 3C, D). Thus, PEDF might regulate the ferroptosis rather than apoptosis or necroptosis in RPE cells.

We further examined the characteristics of ferroptosis in the RPE and choroid tissues of PEDF-knockout mice. The result of TEM showed that RPE cells extracted from PEDF-knockout mice exhibited distinctive morphological features such as smaller mitochondria with decreased membrane density (Fig. 4A). We also observed that the ferroptosis suppressors GPX4 and FTH1 were decreased in PEDF-knockout mouse retinas, as shown by IF assays (Fig. 4B, C). The western blot results showed that GPX4 and FTH1 protein levels were decreased in the RPE and choroidal tissues and retinas of PEDF-KO mice (Fig. 4D–G).

We also cultured primary RPE cells from WT and PEDF-knockout mice. Compared with those of primary RPE cells isolated from WT mice, lipid ROS levels were increased in primary RPE cells isolated from PEDF-knockout mice (Fig. 4H). In addition, the viability of cells isolated from WT mice was better than that of cells isolated from PEDF-KO mice (Fig. 4I). Western blotting and qRT-PCR showed alterations in FTH1 and GPX4 in PEDF-knockout primary RPE cells (Fig. 4J–L). Thus, PEDF deficiency triggers ferroptosis in RPE cells.

PEDF exerted potent antiferroptotic effects on RPE cells

We then used ARPE-19 cells to explore the mechanism of PEDF in the regulation of ferroptosis. First, we used PEDF overexpression adenovirus to infect ARPE-19

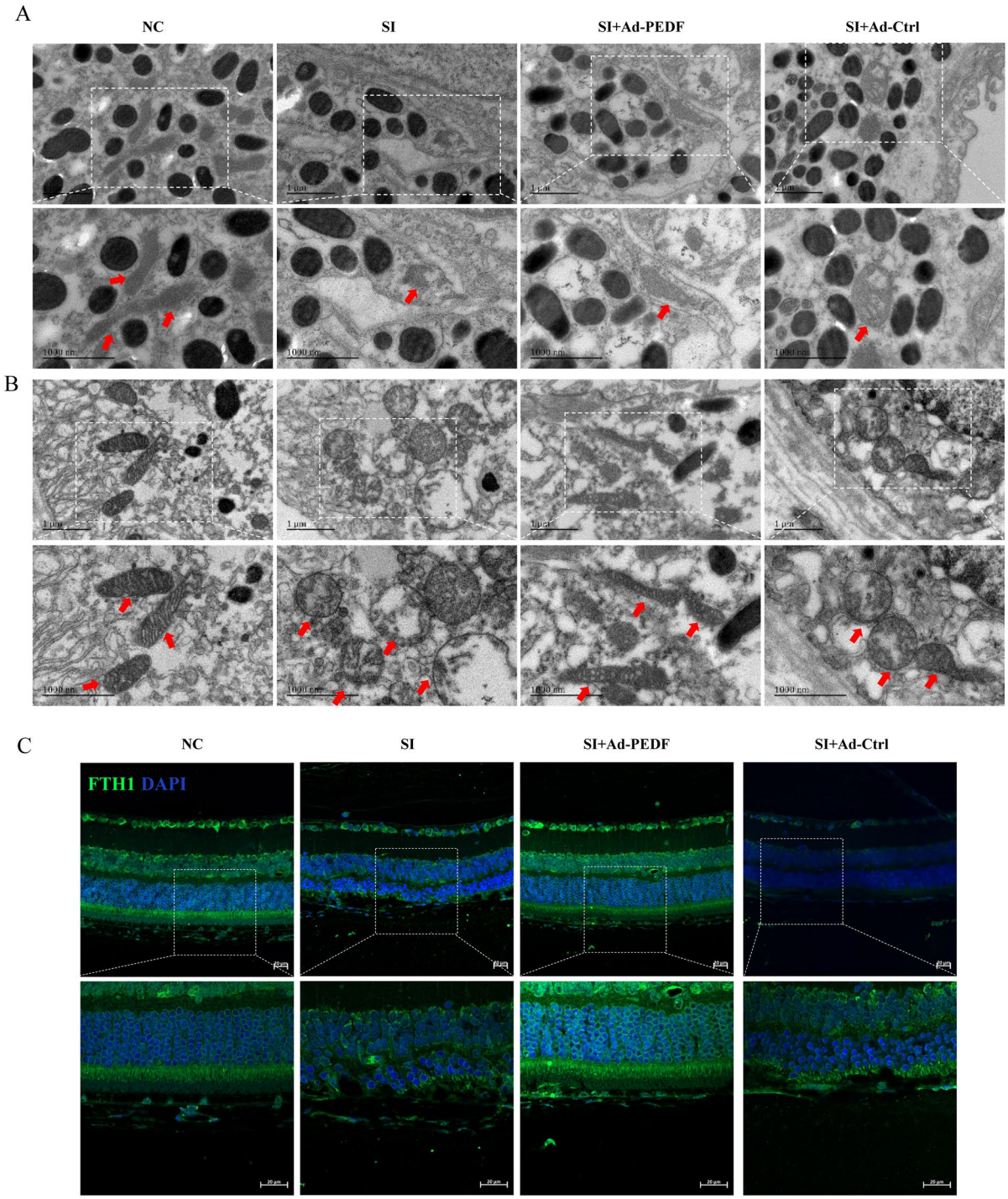

Fig. 7 The overexpression of PEDF inhibited ferroptosis in SI-treated mice. **A**, **B** Ultrastructure of mitochondria in mRPEs from mice after injection with PEDF-expressing adenovirus and/or SI was imaged by TEM. Red arrowheads: mitochondria. Scale bars = 1 μm. **C**–**E** FTH1 (green) (**C**), GPX4 (green) (**D**), and PEDF (red) (**E**) immunostaining of retinas from mice in different treatment groups. Scale bar = 20 μm. **F** Western blot analysis of PEDF, GPX4, and FTH1 in PEDF-expressing RPE-choroids from mice in different treatment groups. **G** Quantification of the PEDF, FTH1, and GPX4 expression in different treatment groups. $^{*}P < 0.05$, $^{**}P < 0.01$, $^{***}P < 0.001$

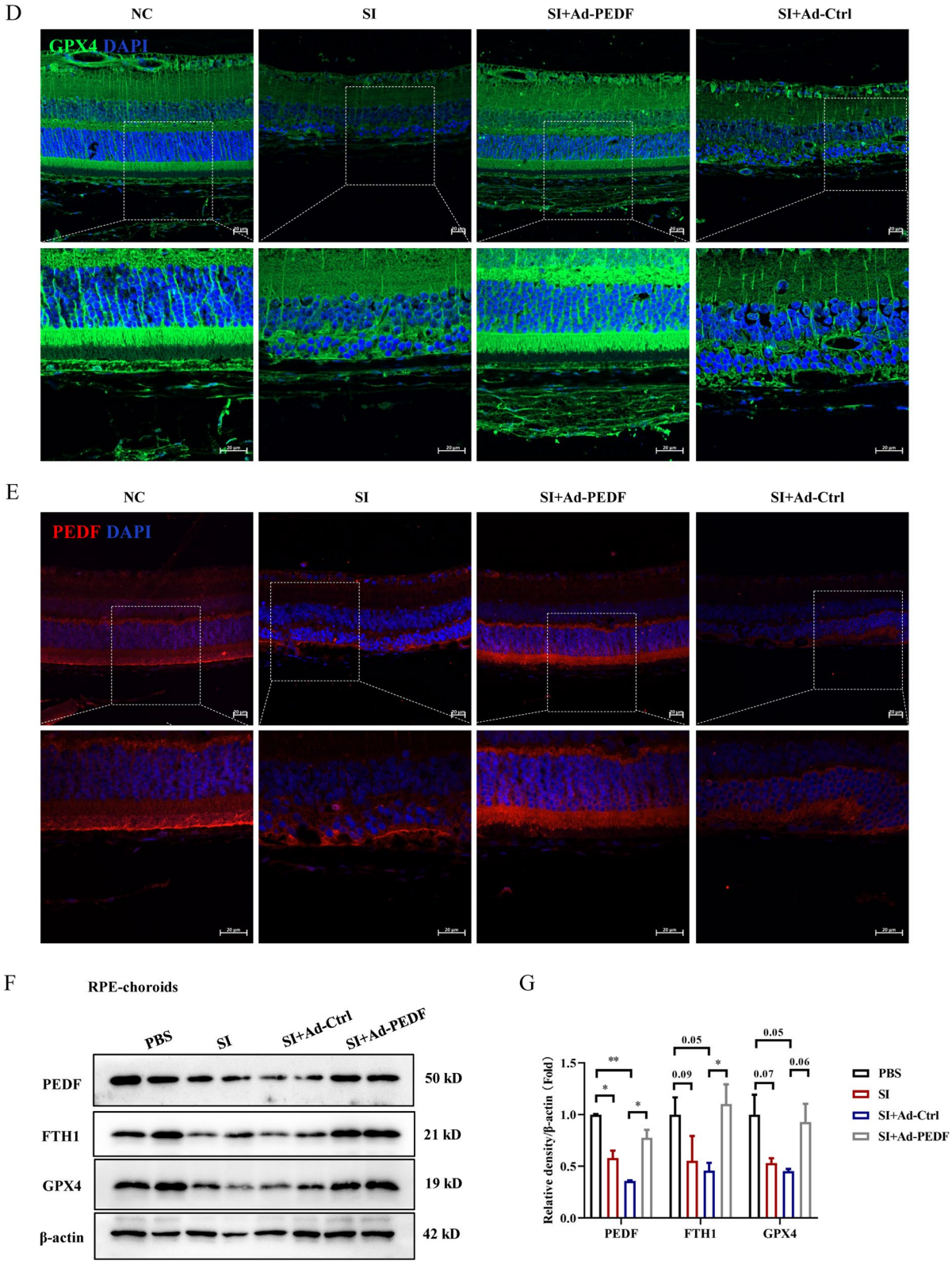

Fig. 7 (continued)

cells (Fig. 5A, B). PEDF overexpression protected against SI-induced acute oxidative death in ARPE-19 cells, as demonstrated by CCK-8 assays (Fig. 5C, D). Brightfield imaging also confirmed the cytoprotective effect of PEDF (Fig. 5E). Furthermore, BODIPY™ 581/591 C11 was used to examine the levels of intracellular and membrane lipid ROS. The results showed that PEDF efficiently decreased the levels of lipid ROS in the presence of SI (Fig. 5F). Western blot analysis showed alterations in FTH1 and GPX4 in SI-treated A19-PEDF cells (Fig. 5G, H). These results indicated that PEDF exerted potent antiferroptotic effects on RPE cells.

PEDF ameliorated SI-induced AMD-like retinopathy

Given the potent protective role of PEDF, we further examined its potential as a treatment for dry AMD in vivo. SI was injected into the tail vein of a mouse model of AMD, and the PEDF adenovirus (Ad-PEDF) or control adenovirus (Ad-Ctrl) was injected intravitreally. The schematic of the process is shown in Fig. 6A. To further evaluate the physiological function of the retinas after tail vein injection of SI, we performed OCT in each group. The OCT results showed that SI injection caused thinning of the retinal layer, which was alleviated in the PEDF overexpression group (Fig. 6B, C). An ERG test was also performed to detect the scotopic response of the retina. After SI injection, the amplitudes of the a-waves and b-waves were decreased (Fig. 6D, E). However, SI mice that were administered the PEDF adenovirus by intravitreal injection showed a relatively excellent response to light stimuli (Fig. 6D, E). We also performed fundus photography to examine whether there were drusen in the mouse retina. The fundus images indicated that SI-treated mice that were intravitreally injected with the PEDF adenovirus had alleviated signs of drusen compared with SI-treated mice that were intravitreally injected with the control adenovirus (Fig. 6F, G). H&E staining showed that PEDF overexpression irregularly reduced RPE cell arrangement (Fig. 6H). SI induced severe retinal damage, while PEDF overexpression significantly attenuated retinal damage. To further elucidate the protective effect of PEDF on RPE cells, we tested the expression of the tight junction protein zonula occludens protein 1 (ZO-1). IF staining showed that tight junctions were impaired in SI-treated ARPE-19 cells but restored by PEDF overexpression (Fig. 6I). Taken together, the in vivo results indicated that PEDF protected the physiological function of the retina.

PEDF overexpression inhibited ferroptosis in the mouse retina

Given the amelioration of symptoms in SI mice that were intravitreally administered the PEDF adenovirus, we also examined the levels of ferroptosis in the retina. TEM confirmed that the mitochondria were smaller and had increased membrane density in RPE and choroidal tissue in SI mice. Furthermore, PEDF overexpression reversed the characteristic morphological features of mitochondria (Fig. 7A, B). In addition, the IF results showed that PEDF significantly increased the expression of GPX4 and FTH1 compared with that in SI-induced mice (Fig. 7C–E). Western blot analysis showed that PEDF restored the expression of FTH1 and GPX4 in RPE and choroidal tissues in SI-treated mice (Fig. 7F, G).

These in vivo and in vitro results showed that PEDF had a potent antiferroptotic effect and could inhibit oxidative stress and maintain mitochondrial homeostasis in RPE cells.

Discussion

This study identified that PEDF could inhibit SI-induced ferroptosis. Our results showed that in SI-treated mice and PEDF-knockout mice, dry AMD-like drusen and retinal atrophy were observed and accompanied by the downregulation of PEDF expression. The restoration of PEDF expression could prevent SI-induced retinal atrophy and RPE dysfunction in mice. During this process, the retinal pigment epithelium was an important target of PEDF because our results showed that PEDF prevented lipid peroxidation and reduced the level of ferroptosis in primary RPE cells and the ARPE-19 cell line, thus protecting barrier function. Overall, our findings suggest that PEDF might be a potential therapeutic target for dry AMD that inhibits ferroptosis in RPE cells.

RPE dysfunction during aging is critical to the pathogenesis of AMD [18]. Previous studies have shown that apoptosis and pyroptosis cause RPE injury, but targeting apoptosis or pyroptosis could not exert a therapeutic effect on AMD [19–21]. Ferroptosis is a novel cell death pathway, and iron overload and lipid peroxidation during the ageing

process are the basis of ferroptosis [22]. Therefore, ferroptosis is more closely associated with age-related degenerative diseases than apoptosis or pyroptosis [23]. Previous studies have shown that in SI-treated mice, ferroptosis is activated in the retina, and the retinal pigment epithelium is injured, resulting in AMD-like pathology [24]. Consistent pathological changes were observed in our SI-treated mouse model. However, how to effectively protect the retinal pigment epithelium from injury and slow the progression of AMD pathology remains unknown.

PEDF is an endogenous protein that is abundantly expressed in normal RPE cells and has an excellent biological safety profile [25]. In addition, PEDF is a multifunctional protein that has been shown to have anti-neovascular [26], anti-inflammatory [27], antifibrotic [28], and neuroprotective [29] functions, and it may play an essential role in maintaining the normal function of the retinal pigment epithelium. In our study, SI-induced dry AMD model mice exhibited downregulated PEDF expression in the retina compared to those in the normal control group, and PEDF-knockout mice exhibited typical AMD-like pathological changes, indicating a potentially important role of PEDF downregulation in the development of AMD. Further experiments demonstrated that the restoration of PEDF prevented retinal atrophy and visual functional damage in SI-treated mice. To elucidate the specific mechanism underlying the protective effect of PEDF, we treated RPE cells and PEDF-overexpressing RPE cells with a specific ferroptosis activator (erastin). The results demonstrated that PEDF overexpression could protect RPE cells from damage caused by the activation of ferroptosis (Fig. 3C, D). Therefore, our study discovered a novel function of PEDF-mediated inhibition of ferroptosis, which provides a reference for the use of PEDF to treat other ferroptosis-related diseases.

The limitations of our study should also be considered. First, the mechanism underlying the downregulation of PEDF in AMD remains unclear. Our results suggested that in SI-treated RPE cells, in addition to the protein level, the transcription level of PEDF was also significantly downregulated. However, the specific molecules and mechanisms that lead to the downregulation of PEDF require further investigation. Revealing the upstream mechanisms of the downregulation of PEDF will help to identify earlier targets for the treatment of AMD. Second, it has been reported that PEDF exerts a protective effect on other retinal cells, such as photoreceptors [30]. In future studies, we will reveal the additional effector cells of PEDF in the retina to optimize its targeted delivery.

Conclusions

In summary, we demonstrated the regulatory role of PEDF in ferroptosis for the first time. Supplementation with PEDF might inhibit ferroptosis, protect RPE cells, and prevent further progression of AMD.

Abbreviations *AMD*: Age-related macular degeneration; *RPE*: Retinal pigment epithelium; *SI*: Sodium iodate; *PEDF*: Pigment epithelial-derived factor; *FTH1*: Ferritin heavy chain 1; *GPX4*: glutathione peroxidase 4; *ERG*: Electroretinography; *H&E*: Hematoxylin and eosin; *OCT*: Optical coherence tomography; *qRT-PCR*: Quantitative real-time PCR; *TEM*: Transmission electron microscope; *ROS*: Reactive oxygen species; *IF*: Immunofluorescence; *CCK-8*: Cell Counting Kit-8; *FBS*: Fetal bovine serum; *ZO-1*: Zonula occludens protein 1

Author contribution KBL, LHL and WX conceived the study and designed the experiments. WX and LHL performed the experiments, finalized the data set, and drafted the manuscript. WX and LHL contributed equally in this study. QZ participated in the experiments, preparation the resources and revised the original draft. YCZ, JHS, and ZTC contributed to the in vivo experiments. GQG, and KBL participated in the discussion. KBL supervised the entire study and revised the manuscript. All authors read and approved the final manuscript.

Funding This work was supported by National Natural Science Foundation of China (82171066). This article was also supported by Natural Science Foundation of Guangdong Province (2414050005730), so we added this funding in this version. Guangzhou Science and Technology Plan Project (202102010333 and SL2024A03J00359), and Guangdong Basic and Applied Basic Research Fund Project (2021A1515010895 and SL2023A04J00138).

Data Availability The experimental data reported in this study will be made available upon reasonable request from the corresponding author (laikunbei888@mail.sysu.edu.cn).

Declarations

Competing interests The authors declare no competing interests.

References

1. Fleckenstein M, Keenan TDL, Guymer RH, Chakravarthy U, Schmitz-Valckenberg S, Klaver CC, et al. Age-related macular degeneration. Nat Rev Dis Primers. 2021;7(1):31.
2. Blasiak J, Sobczuk P, Pawlowska E, Kaarniranta K. Interplay between aging and other factors of the pathogenesis of age-related macular degeneration. Ageing Res Rev. 2022;81:101735.
3. Sharma R, Bose D, Maminishkis A, Bharti K. Retinal pigment epithelium replacement therapy for age-related macular degeneration: are we there yet? Annu Rev Pharmacol Toxicol. 2020;60:553–72.
4. Tang Z, Ju Y, Dai X, Ni N, Liu Y, Zhang D, et al. HO-1-mediated ferroptosis as a target for protection against retinal pigment epithelium degeneration. Redox Biol. 2021;43:101971.
5. Sun Y, Zheng Y, Wang C, Liu Y. Glutathione depletion induces ferroptosis, autophagy, and premature cell senescence in retinal pigment epithelial cells. Cell Death Dis. 2018;9(7):753.
6. Gupta U, Ghosh S, Wallace CT, Shang P, Xin Y, Nair AP, et al. Increased LCN2 (lipocalin 2) in the RPE decreases autophagy and activates inflammasome-ferroptosis processes in a mouse model of dry AMD. Autophagy. 2022;1–20.
7. Stockwell BR. Ferroptosis turns 10: Emerging mechanisms, physiological functions, and therapeutic applications. Cell. 2022;185(14):2401–21.
8. Ouyang S, You J, Zhi C, Li P, Lin X, Tan X, et al. Ferroptosis: the potential value target in atherosclerosis. Cell Death Dis. 2021;12(8):782.
9. Zhao T, Guo X, Sun Y. Iron accumulation and lipid peroxidation in the aging retina: implication of ferroptosis in age-related macular degeneration. Aging Dis. 2021;12(2):529–51.
10. Ma B, Zhou Y, Liu R, Zhang K, Yang T, Hu C, et al. Pigment epithelium-derived factor (PEDF) plays anti-inflammatory roles in the pathogenesis of dry eye disease. Ocul Surf. 2021;20:70–85.
11. Barnstable CJ, Tombran-Tink J. Neuroprotective and antiangiogenic actions of PEDF in the eye: molecular targets and therapeutic potential. Prog Retin Eye Res. 2004;23(5):561–77.
12. Ding DC, Wen YT, Tsai RK. Pigment epithelium-derived factor from ARPE19 promotes proliferation and inhibits apoptosis of human umbilical mesenchymal stem cells in serum-free medium. Exp Mol Med. 2017;49(12):e411.
13. Carpino G, Cardinale V, Di Giamberardino A, Overi D, Donsante S, Colasanti T, et al. Thrombospondin 1 and 2 along with PEDF inhibit angiogenesis and promote lymphangiogenesis in intrahepatic cholangiocarcinoma. J Hepatol. 2021;75(6):1377–86.
14. He X, Cheng R, Park K, Benyajati S, Moiseyev G, Sun C, et al. Pigment epithelium-derived factor, a noninhibitory serine protease inhibitor, is renoprotective by inhibiting the Wnt pathway. Kidney Int. 2017;91(3):642–57.
15. Wang B, Wang L, Gu S, Yu Y, Huang H, Mo K, et al. D609 protects retinal pigmented epithelium as a potential therapy for age-related macular degeneration. Signal Transduct Target Ther. 2020;5(1):20.
16. Chan CM, Huang DY, Sekar P, Hsu SH, Lin WW. Reactive oxygen species-dependent mitochondrial dynamics and autophagy confer protective effects in retinal pigment epithelial cells against sodium iodate-induced cell death. J Biomed Sci. 2019;26(1):40.
17. Tang Z, Huo M, Ju Y, Dai X, Ni N, Liu Y, et al. Nanoprotection against retinal pigment epithelium degeneration via ferroptosis inhibition. Small Methods. 2021;5(12):e2100848.
18. Datta S, Cano M, Ebrahimi K, Wang L, Handa JT. The impact of oxidative stress and inflammation on RPE degeneration in non-neovascular AMD. Prog Retin Eye Res. 2017;60:201–18.
19. Cai J, Nelson KC, Wu M, Sternberg P, Jones DP. Oxidative damage and protection of the RPE. Prog Retin Eye Res. 2000;19(2):205–21.
20. Tseng WA, Thein T, Kinnunen K, Lashkari K, Gregory MS, D'Amore PA, et al. NLRP3 inflammasome activation in retinal pigment epithelial cells by lysosomal destabilization: implications for age-related macular degeneration. Invest Ophthalmol Vis Sci. 2013;54(1):110–20.
21. Eisenstein M. The quest to treat dry age-related macular degeneration. Nature. 2021;600(7887):S1.
22. Stockwell BR, Friedmann Angeli JP, Bayir H, Bush AI, Conrad M, Dixon SJ, et al. Ferroptosis: a regulated cell death nexus linking metabolism, redox biology, and disease. Cell. 2017;171(2):273–85.
23. Ru Q, Li Y, Xie W, Ding Y, Chen L, Xu G, et al. Fighting age-related orthopedic diseases: focusing on ferroptosis. Bone Res. 2023;11(1):12.
24. Yang M, Tsui MG, Tsang JKW, Goit RK, Yao K-M, So K-F, et al. Involvement of FSP1-CoQ10-NADH and GSH-GPx-4 pathways in retinal pigment epithelium ferroptosis. Cell Death Dis. 2022;13(5):468.
25. Becerra SP, Notario V. The effects of PEDF on cancer biology: mechanisms of action and therapeutic potential. Nat Rev Cancer. 2013;13(4):258–71.
26. Ho TC, Chen SL, Yang YC, Liao CL, Cheng HC, Tsao YP. PEDF induces p53-mediated apoptosis through PPAR gamma signaling in human umbilical vein endothelial cells. Cardiovasc Res. 2007;76(2):213–23.
27. Yamagishi S-I, Matsui T, Adachi H, Takeuchi M. Positive association of circulating levels of advanced glycation end products

(AGEs) with pigment epithelium-derived factor (PEDF) in a general population. Pharmacol Res. 2010;61(2):103–7.
28. Xiang W, Li L, Hong F, Zeng Y, Zhang J, Xie J, et al. N-cadherin cleavage: a critical function that induces diabetic retinopathy fibrosis via regulation of β-catenin translocation. FASEB J. 2023;37(4):e22878.
29. Tombran-Tink J, Barnstable CJ. PEDF: a multifaceted neurotrophic factor. Nat Rev Neurosci. 2003;4(8):628–36.
30. Comitato A, Subramanian P, Turchiano G, Montanari M, Becerra SP, Marigo V. Pigment epithelium-derived factor hinders photoreceptor cell death by reducing intracellular calcium in the degenerating retina. Cell Death Dis. 2018;9(5):560.